

Article

The Influence of the Mineralogical Composition of Ultramafic Rocks on Their Engineering Performance: A Case Study from the Veria-Naousa and Gerania Ophiolite Complexes (Greece)

Panagiota P. Giannakopoulou ^{1,*}, Petros Petrounias ¹ , Aikaterini Rogkala ¹, Basilios Tsikouras ² , Panagiotis M. Stamatis ¹ , Panagiotis Pomonis ³ and Konstantin Hatzipanagiotou ¹

¹ Department of Geology, Section of Earth Materials, University of Patras, 265 04 Patras, Greece; Geo.plan@outlook.com (P.P.); krogkala@upatras.gr (A.R.); panayiotisstamatis@gmail.com (P.M.S.); k.hatzipanagiotou@upatras.gr (K.H.)

² Faculty of Science, Physical and Geological Sciences, Universiti Brunei Darussalam, Jalan Tungku Link, Gadong, Bandar Seri Begawan BE1410, Brunei Darussalam; basilios.tsikouras@ubd.edu.bn

³ Department of Geology and Geoenvironment, National and Kapodistrian University of Athens, Panepistimioupolis Zografou, 157 84 Athens, Greece; ppomonis@geol.uoa.gr

* Correspondence: peny_giannakopoulou@windowslive.com

Received: 29 May 2018; Accepted: 6 July 2018; Published: 9 July 2018



Abstract: This case study investigates the influence of the mineralogical composition of ultramafic rocks derived from two ophiolite complexes from Greece (Veria-Naousa and Gerania) on their mechanical, physical and physicochemical properties. The investigated lithologies include lherzolite, harzburgite, dunite and olivine-orthopyroxenite with variable degrees of alteration. The ratio of secondary minerals to primary minerals (SEC/PR) of the studied ultramafic rocks shows good correlations with their physical, physicochemical and mechanical properties, suggesting that alteration has a negative effect on the engineering performance of the ultramafic rocks. Among the secondary minerals, serpentine plays the most critical role in determining the moisture content, the total porosity and hence the soundness of the host rocks, due to its phyllosilicate structure, which allows more water/solutions to be captured. The high percentage of serpentine creates surfaces of weakness, and as a result, it decreases the rock strength. The low microtopography of highly serpentinized rocks results in their reduced mechanical performance.

Keywords: peridotite; serpentine; aggregates; engineering properties

1. Introduction

Ophiolitic rocks are remnants of the Earth's oceanic crust and upper mantle, derived from mid-ocean ridges or marginal basins [1]. Generally, a complete ophiolite suite consists of ultramafic, mafic, hypabyssal and extrusive rocks. Research of the properties of ophiolitic rocks for industrial and constructive purposes shows an increasing interest. Ophiolitic rocks are used extensively as engineering materials, including aggregates for road construction, concrete and railway ballast [2–5]. The suitability of aggregates for their applications is determined by evaluating their physical, physicochemical and mechanical properties, which are collectively known as engineering properties.

The engineering properties of rocks mainly depend on their mineralogical composition, textural characteristics, degree of chemical alteration, weathering and deformation [2,4–10]. Strong to very strong interrelationships among engineering properties of ultramafic rocks have been documented and studied by Petrounias et al. [4] and Giannakopoulou et al. [10]. Several researchers have been focused

on the effect of different mineralogical phases on the mechanical properties of rocks. Tandon and Gupta [11] have strongly correlated the quartz content with the uniaxial compressive strength (UCS) results of volcanic rocks. Ündül [12] has correlated the biotite content with the UCS results of andesites. Cowie et al. [13] has strongly correlated the mica content with the Brazilian test (BTS) of granites. The soundness test of the magnesium sulphate heptahydrate is considered to be suitable for the investigation of the durability of coarse aggregates. This test, in conjunction with other methods, such as UCS and Los Angeles abrasion (LA), may lead to a reliable appreciation of aggregate durability [14]. Ultramafic rocks exhibit a wide range of compositions, as well as of mineralogical and textural features; thus, the existence of lithotypes with variable engineering properties is very common even in the same suite. The mineralogical features, textures and lithological properties of rocks change due to their alteration, and thus their engineering properties may show large variations.

The influence of alteration phenomena on the performance of aggregates has been investigated by many researchers. Studies have mostly been concentrated on granitic rocks [15,16]; however, several authors have conducted analogous researches in acidic-intermediate volcanic rocks [17,18], metamorphic rocks [19,20], as well as mafic [2,21] and ultramafic rocks [21–24]. Alteration affects may be critical as increased percentages of certain secondary minerals, such as serpentine and talc, affecting negatively the mechanical properties of ultramafic aggregates, due to their smooth layers, cleavage and platy or fibrous crystal habit [22,23].

Serpentinization is the most common alteration process in ultramafic rocks in the ocean floor or subduction zones [1,25]. First-order changes of the major element composition of peridotites induced by serpentinization are the addition of 10–12 wt % water and loss of CaO [25–27]. Density decreases from about $3.3 \text{ g}\cdot\text{cm}^{-3}$ to as low as $2.55 \text{ g}\cdot\text{cm}^{-3}$ [28], the volume increases and the rock becomes weaker [1,29], with wide-ranging and significant tectonic consequences [30–32].

The goal of this paper is to elucidate how the mineralogical composition of ultramafic rocks influences their engineering performance using a combination of petrographic methods and laboratory tests. In this case study, we use ultramafic samples from two ophiolite complexes in Greece, Veria-Naousa and Gerania, which show an extensive range of serpentinization.

2. Geological Setting

Forty-two ultramafic hand specimens were collected for petrographic investigation; twenty-two of them were from the Veria-Naousa ophiolite complex (Central Macedonia District), and twenty were from the Gerania ophiolite complex (Corinthos District). Eighteen representative block samples (80–120 kg in weight for each) were additionally collected for the determination of their engineering parameters; seven of them were from the Veria-Naousa ophiolite complex (Central Macedonia District), and eleven of them were from the Gerania ophiolite complex (Corinthos District). After extensive field mapping and petrographic observations, the existing geological maps were modified by using the GIS software (ArcMap 10.1).

2.1. The Veria-Naousa Ophiolite Complex

The Veria-Naousa ophiolite complex, located in Northern Greece, belongs to the Almopias subzone of the Axios geotectonic zone (Figure 1). In this ophiolite complex, serpentinized lherzolite and harzburgite, crosscut by scarce pyroxenitic dykes, occur together with gabbro, diabase and pillow basalt, which are considered to be remnants of oceanic lithosphere that have been placed onto Late Triassic–Jurassic platform carbonates of the Pelagonian Zone, from Upper Jurassic to Lower Cretaceous [33–36]. The serpentinized peridotites are characterized by high tectonic stress, expressed by an intense network of joints. Rare rodingite dykes occur in these ultramafic rocks. Conglomeratic limestones and flysch and breccia limestone of Neogene to Quaternary age lie uncomfortably on the ophiolitic rocks. Granite to granodiorite intrusions are also present. The eastern contact of the ophiolite with the Pelagonian carbonates is dominated by a cataclastic zone of diabasic fragments and albitite

cement. Pliocene volcanic rocks of the Almopias subzone ranging in composition from trachyte to andesite occur to the east of the ophiolitic complex.

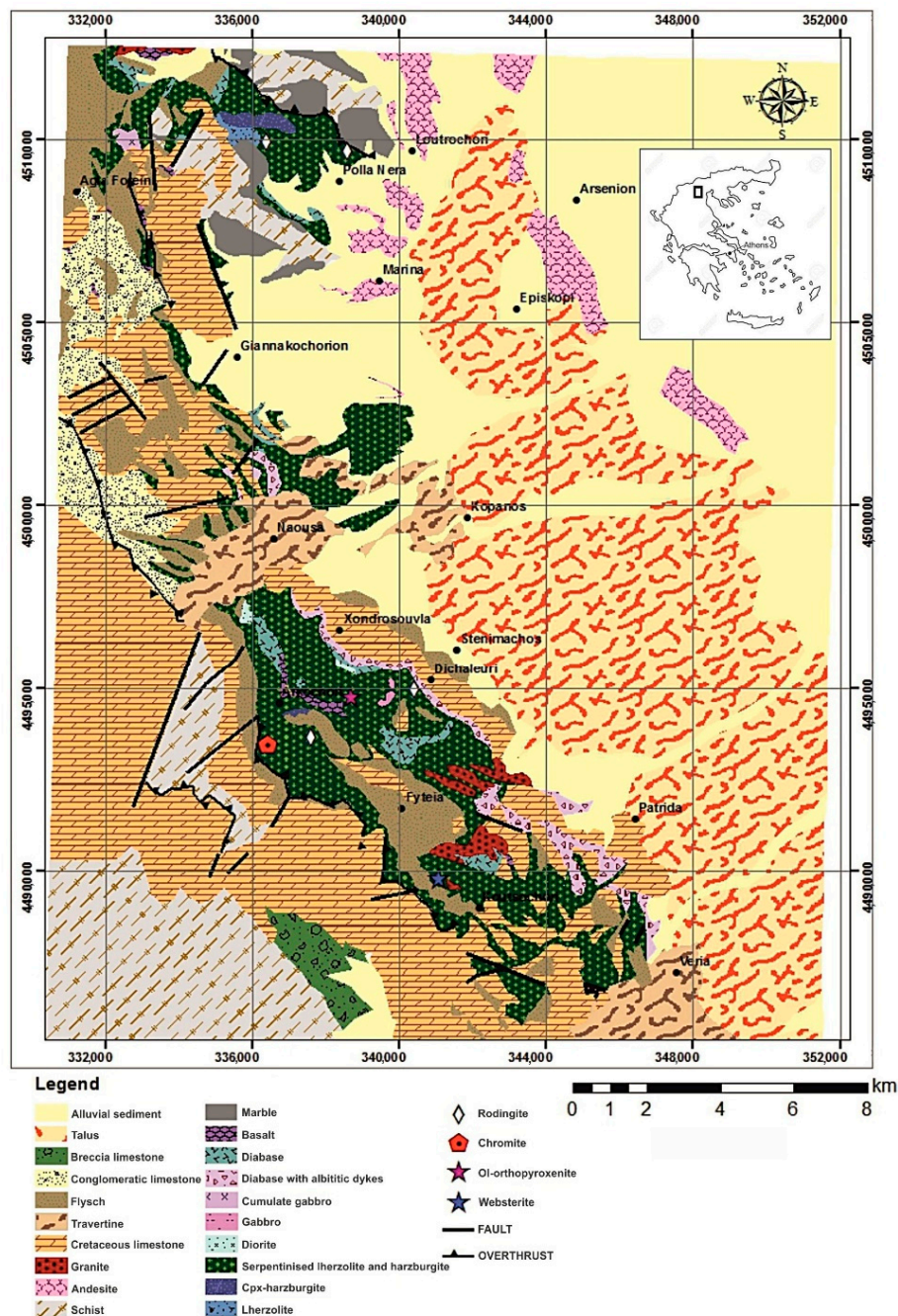


Figure 1. Geological map of the Veria-Naousa region [5,37] (modified after fieldwork and mapping by using ArcMap 10.1); the rectangle in the inset shows the study area.

2.2. The Gerania Ophiolite Complex

Gerania Mountains belong to the Pelagonian geotectonic zone of the internal Hellenides. They comprise a Permian sedimentary and volcanic succession overlain by a series of carbonate rocks and lesser radiolarites [38–42]. This succession is tectonically overlain by an ophiolite sequence. The ophiolite is a NE-trending rhomb-shaped outcrop, with approximately 10 km in length and 5 km in width, representing an incomplete and dismembered ophiolite sequence. It is dominated by variably

serpentinized and tectonized lherzolite, locally crosscut by thin pyroxenite dykes with subordinate harzburgite and dunite (Figure 2). These serpentinized peridotites are interrupted by gabbro dykes, some of which have been transformed into rodingites. An ophiolite mélangé includes fragments of lavas, serpentinized peridotites, gabbros, oceanic sediments previously described as schist-chert formation [39], as well as an amphibolite metamorphic sole tectonically underlie the ophiolite.

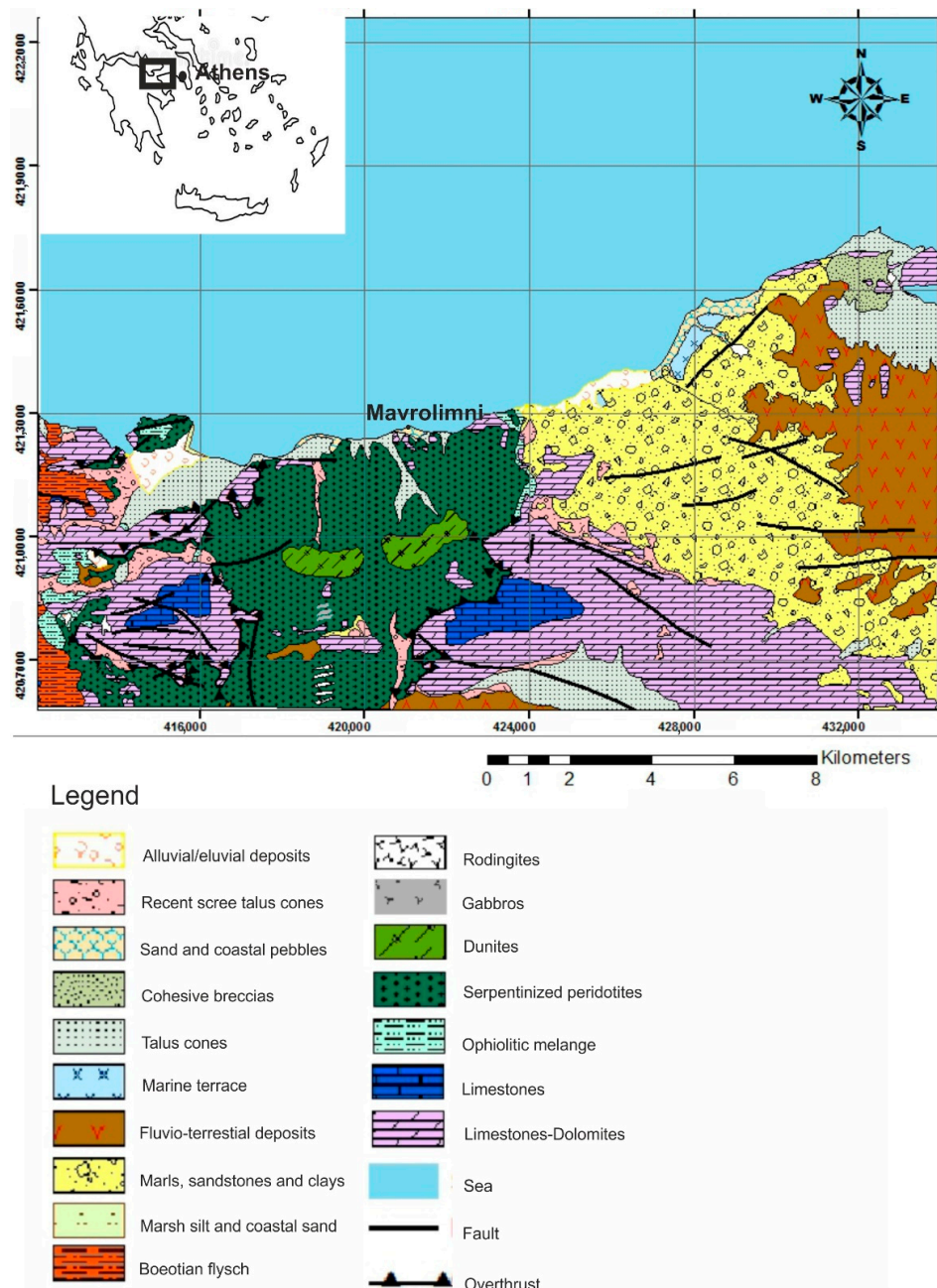


Figure 2. Geological map of the Gerania region [10,39] (modified after fieldwork and mapping by using ArcMap 10.1); the rectangle in the inset shows the study area.

3. Materials and Methods

Eighteen block samples of ultramafic rocks were collected according to the EN 932-1 [43] standard to evaluate their suitability as aggregates for construction applications, and they have been petrographically observed using a combination of petrographic methods. The mineralogical

and textural characteristics of the samples were studied in 60 polished-thin sections (42 of them were prepared from regular hand specimens and 18 were prepared from the block samples) in a polarizing optical microscope (Leitz Ortholux II POL-BK Ltd., Midland, ON, Canada), according to the EN-932-3 [44] standard for the petrographic description of aggregates, and a scanning electron microscope (SEM). Mineralogical composition was also determined with the aid of the Rietveld method after powder X-ray Diffractometry (XRD) using a Bruker D8 Advance diffractometer, with Ni-filtered $\text{CuK}\alpha$ radiation. Random powder mounts were prepared by gently pressing the powder into the cavity holder. The scanning area for bulk mineralogy of the specimens covered the 2θ interval ($2\text{--}70^\circ$), with a scanning angle step size of 0.015° and a time step of 0.1 s. The mineral phases were determined using the DIFFRACplus EVA 12[®] software (Bruker-AXS, Bierica, MA, USA) based on the ICDD Powder Diffraction File of PDF-2 2006, while the semi-quantitative analyses were performed by TOPAS 3.0[®] software, based on the Rietveld method refinement routine. The routine is based on the calculation of a single mineral-phase pattern according to the crystalline structure of the respective mineral, and the refinement of the pattern using a non-linear least squares routine. The quantification errors calculated for each phase according to Bish and Post [45] are estimated to be ~1%, while the detection limit is 2%.

The surface texture of aggregate particles was studied in secondary electron images (SEI) according to BS 812 Part 1 [46].

The engineering properties of the ultramafic rocks were determined in the Research Laboratory of Minerals and Rocks, Department of Geology, University of Patras, Patra, Greece. Moisture content (w) was measured in accordance to the AASHTO T-255 [47] standard; total porosity (n_t) was determined according to the ISRM 1981 [48] standard; the LA test was carried out in accordance to the ASTM C-131 [49] standard using the “B” gradation; and the soundness test (S) was elaborated according to the EN 1367-2 [50] standard. The UCS was determined from the average value of six cylindrical rock specimens for each sample with diameters ranging from 51 to 54 mm and their height/diameter ratios between two and three for each sample (ASTM D-2938 [51]). The point load test [$I_{s(50)}$] is broadly used to determine the UCS indirectly, due to its ease of testing, low cost and possible field applications. This test was performed in three cylindrical specimens for each block sample, with a length-to-diameter ratio larger than 1. The cylindrical specimens were stressed diametrically until breakage according to I.S.R.M, 1985 [52].

4. Results

4.1. Petrographic Features

4.1.1. Microscopic Observations

Serpentinized peridotites from the Veria-Naousa ophiolite complex are characterized by mesh and local bastitic or cataclastic textures. The primary mineralogical assemblage of serpentinized lherzolite has been mostly obliterated by alteration and only a few relics of olivine, orthopyroxene, clinopyroxene and spinel (Al-spinel and Cr-spinel) are present (Figure 3a,b). A scarce network of calcite veinlets occurs as well. The primary assemblage of the harzburgite comprises relics of orthopyroxene, rare clinopyroxene, olivine, as well as spinel (magnesiochromite and Cr-spinel). Orthopyroxene appears as subhedral porphyroclasts and most of them show exsolution lamellae of clinopyroxene, a typical feature of mantle peridotites. The existence of intense fragmentation of spinel and the presence of intragranular microcracks indicate brittle deformation. Serpentine consists of the main alteration product, showing mainly mesh, bastitic and interpenetrating textures (Figure 3c,d). Chlorite and magnetite are the minerals, which complete the secondary assemblage of the harzburgite. The ol-orthopyroxenite is the least altered lithology and generally presents coarse, granular to porphyroclastic texture. It consists mainly of orthopyroxene, rare clinopyroxene, olivine and spinel. Orthopyroxenes exhibit local kink bands, undulatory extinction and frequent exsolution lamellae of clinopyroxene (Figure 3e). Serpentine is the dominant alteration product forming mesh texture (Figure 3f). Lesser amounts of chlorite, talc, anthophyllite and magnetite occur [36].

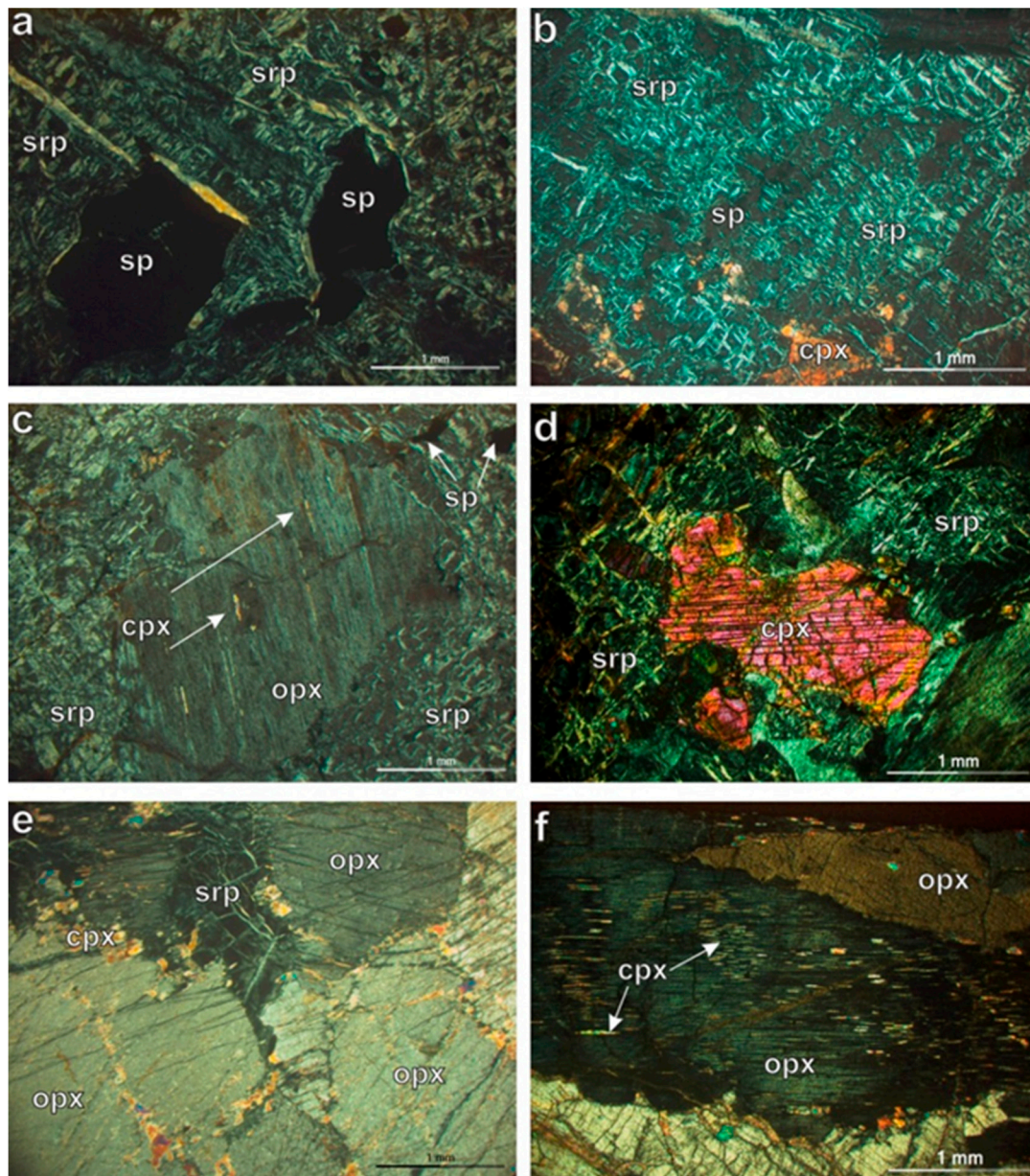


Figure 3. Photomicrographs of: (a) spinels in a mass of serpentine with mesh texture in a serpentinized lherzolite (sample, BE.103B, XPL); (b) relics of clinopyroxene and spinel in mesh serpentine presented in a serpentinized lherzolite (sample BE.102, XPL); (c) serpentine showing bastite formation pseudomorphing orthopyroxene in a serpentinized harzburgite (sample BE.122, XPL); (d) relics of clinopyroxene in interpenetrating serpentine replacing mesh serpentine in a serpentinized harzburgite (sample BE.01B, XPL); (e) porphyroclastic texture with limited presence of serpentine with mesh texture in ol-orthopyroxenite (sample BE.67B, XPL); and (f) exsolution lamellae of clinopyroxene within orthopyroxene of ol-orthopyroxenite (sample BE.67, XPL). Abbreviations: opx: orthopyroxene; cpx: clinopyroxene; srp: serpentine; sp: spinel.

Peridotites from the Gerania ophiolite complex include lherzolite, harzburgite and dunite with low to moderate degrees of serpentinization and deformation. The lherzolite shows protogranular, porphyroclastic and locally cataclastic textures, with the primary assemblage, including olivine, orthopyroxene and clinopyroxene (Figure 4a,b). Opaque minerals (mainly Al-spinel in light brown color) are present in small amounts.

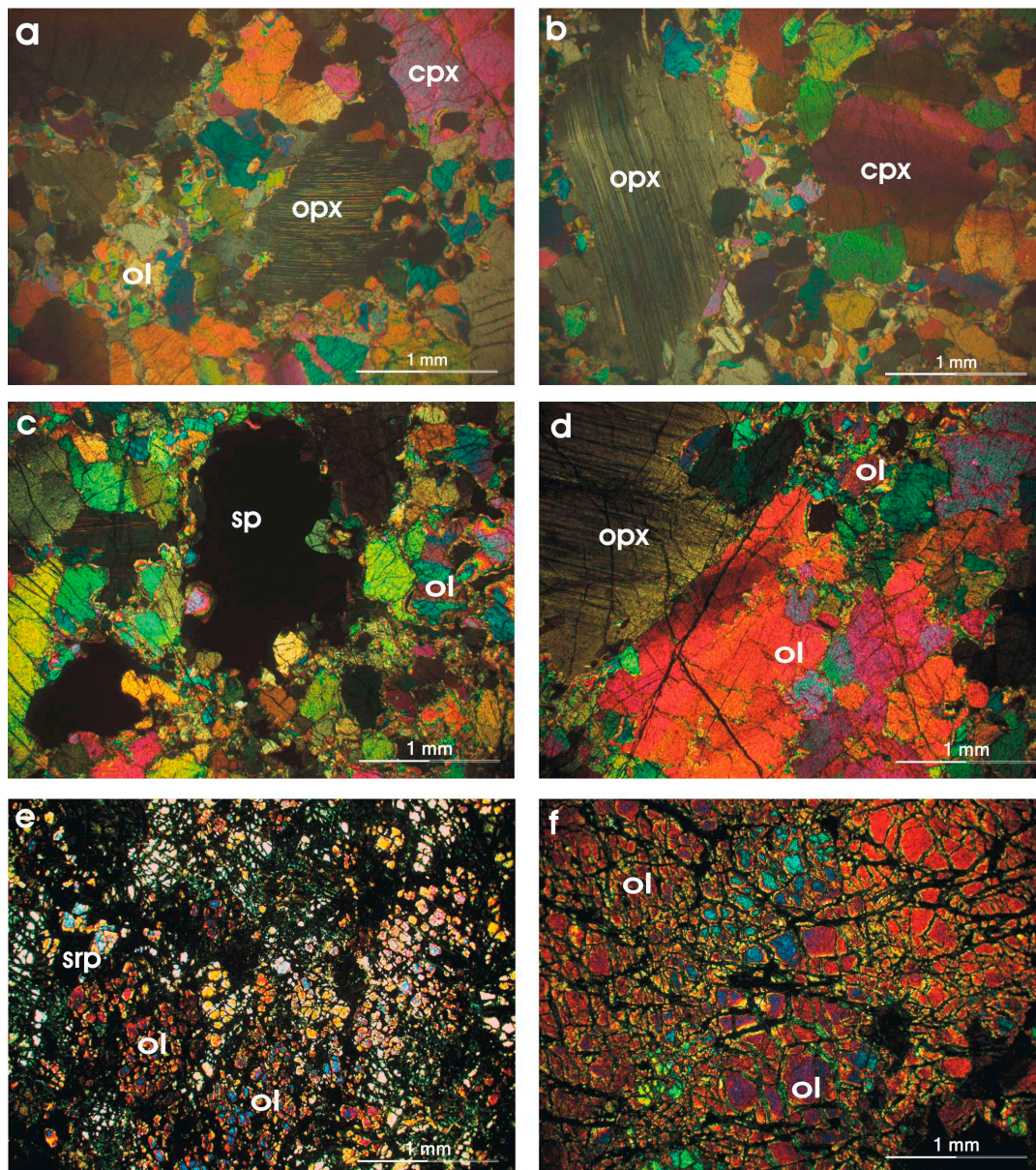


Figure 4. Photomicrographs of: (a,b) porphyroclastic and cataclastic textures of lherzolite with porphyroclasts of orthopyroxenes showing kink banding, crystals of olivine and clinopyroxene showing undulatory extinction (sample GE.25, GE.32, XPL); (c) spinels with embayed margins in cataclastic harzburgite (sample GE.28, XPL); (d) porphyroclasts of orthopyroxene and olivine crystals with undulatory extinction in harzburgite (sample GE.28, XPL); (e) granular texture of fine grained dunite with a low percentage of serpentine (sample GE.17, XPL); and (f) granular texture of dunite (sample GE.34, XPL). Abbreviations: ol: olivine; opx: orthopyroxene; cpx: clinopyroxene; srp: serpentine; sp: spinel.

Porphyroclastic texture is characterized by large orthopyroxene, clinopyroxene and olivine clasts (0.2 mm to 2 mm across) in a finegrained matrix (average grain size <0.2 mm) made up of recrystallized olivine neoblasts (Figure 4a). The largest orthopyroxene clasts display strongly embayed grain boundaries filled with olivine neoblasts (Figure 4a,b). Evidence of high-temperature plastic deformation is shown in strained olivine and orthopyroxene porphyroclasts, which display undulatory extinction, strain lamellae and kink banding (Figure 4b). Serpentine is the main secondary mineral, which shows mostly mesh and locally ribbon textures. The effect of serpentinization also

leads to the replacement of orthopyroxene from bastite. Some orthopyroxene and clinopyroxene crystals are additionally replaced by chlorite and actinolite. A dense network of microcracks is also observed in lherzolite. The harzburgite presents mainly porphyroclastic and locally cataclastic textures (Figure 4c). Its primary assemblage includes olivine, orthopyroxene (most of them with exsolution lamellae of clinopyroxene) and rare clinopyroxene. Olivine appears as porphyroclasts, which present strong deformation (strain lamellae, kink banding and undulose extinction), as well as small-sized unstrained neoblasts (Figure 4d). Frequent replacement of orthopyroxene from olivine neoblasts is also observed. Al-spinel in light brown color and Cr-spinel characterized in red-brown color are present in small amounts, some of which display embayed margins and rims altered to secondary magnetite. A dense network of microcracks also occurs in the harzburgite. The serpentine comprises the most common secondary phase presenting ribbon texture; minor chlorite occurs as well. The dunite presents cataclastic and locally granular texture (Figure 4e,f), whereas the serpentinized samples show mainly mesh, as well as local ribbon and interwoven textures. Primary assemblage includes mostly olivine and scarce relic clasts of orthopyroxene. Infrequent opaque minerals (mainly chromite) are also present. Secondary talc and chlorite occur in minor amounts.

4.1.2. XRD Analysis

Representative XRD patterns from ultramafic studied rock samples are shown below (Figure 5). The bulk compositions (calculated using the Rietveld method) of the tested rock samples are consistent with our petrographic observations under the polarizing microscope where a wide range of the abundance of serpentine was observed, ranging from 3.0% to 78.0% (Table 1).

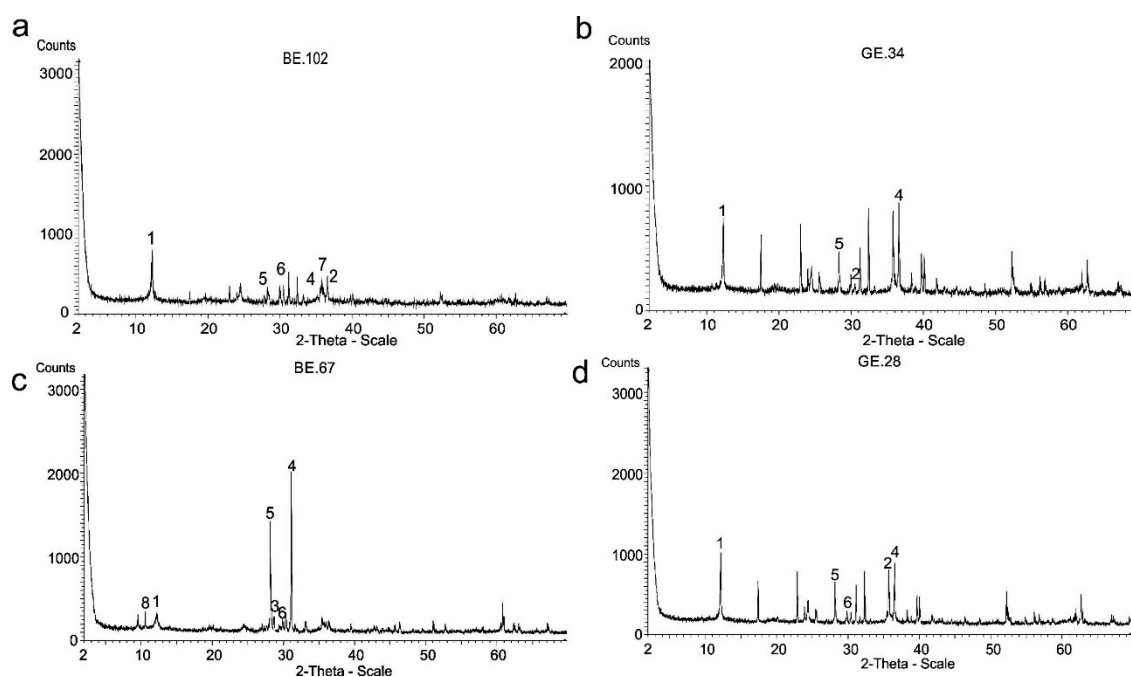


Figure 5. Representative X-ray diffraction patterns of the studied ultramafic rock samples: (a) serpentinized lherzolite; (b) dunite; (c) ol-orthopyroxenite; and (d) harzburgite. Sample numbers are indicated as insets (1: serpentine; 2: spinel; 3: talc; 4: olivine; 5: orthopyroxene; 6: clinopyroxene; 7: magnetite; 8: anthophyllite).

Table 1. Mineralogical composition of the studied rock samples. The quantification errors calculated for each phase according to Bish and Post [45] are estimated to be ~1% (BE: Veria-Naousa ophiolite complex; GE: Gerania ophiolite complex; ol: olivine; opx: orthopyroxene; cpx: clinopyroxene; sp: spinel; mgt: magnetite; ath: anthophyllite; chl: chlorite; talc: talc; bruc: brucite; Srp: serpentine; SEC/PR: ratio of secondary to primary minerals).

Lithology	Samples	ol	opx	cpx	sp	mgt	chl	talc	bruc	ath	Srp	SEC/PR
Serpentinized harzburgite	BE.01B	3.0	9.5	0.0	7.0	2.5	0.0	0.0	0.0	0.0	78.0	4.13
Serpentinized harzburgite	BE.12B	9.6	19.0	2.0	9.5	4.9	0.0	0.0	0.0	0.0	55.0	1.49
Serpentinized lherzolite	BE.102	3.0	11.0	7.0	2.5	1.5	0.0	0.0	0.0	0.0	75.0	3.26
Serpentinized lherzolite	BE.103B	9.0	8.4	6.1	6.5	0.0	0.0	0.0	0.0	0.0	70.0	2.33
Serpentinized harzburgite	BE.122	0.0	11.5	0.0	8.2	3.3	7.8	0.0	0.0	0.0	69.2	4.08
Ol-orthopyroxenite	BE.67	5.0	83.8	9.2	0.0	0.0	0.0	0.0	0.0	0.8	1.2	1.38
Ol-orthopyroxenite	BE.67B	5.4	81.1	12.0	0.0	0.0	0.0	0.0	0.0	0.0	1.5	0.03
Serpentinized dunite	GE.17	40.5	0.0	0.0	1.6	0.0	0.0	0.0	17.9	0.0	40.0	0.92
Lherzolite	GE.25	51.4	19.0	17.9	8.5	0.0	0.0	0.0	0.0	0.0	3.0	0.09
Serpentinized lherzolite	GE.26	18.4	19.0	11.6	3.0	0.0	0.0	0.0	0.0	0.0	48.0	0.05
Harzburgite	GE.28	60.5	24.0	3.89	3.5	1.5	0.0	0.0	0.0	0.0	6.6	0.14
Lherzolite	GE.30	51.4	16.7	17.9	8.7	0.0	0.0	0.0	0.0	0.0	5.2	0.12
Lherzolite	GE.31	46.5	14.6	19.3	7.1	0.0	0.0	2.4	0.0	0.0	10.0	0.05
Lherzolite	GE.32	50.0	16.5	14.0	8.5	0.0	0.0	0.0	0.0	0.0	11.0	0.43
Lherzolite	GE.33	51.4	17.0	17.9	8.5	0.0	0.0	0.0	0.0	0.0	5.0	0.86
Dunite	GE.34	50.0	18.0	0.0	2.0	0.0	0.0	0.0	0.0	0.0	30.0	0.12
Serpentinized dunite	GE.37	43.7	3.9	0.0	6.3	4.6	0.0	6.5	0.0	0.0	35.0	0.01
Lherzolite	GE.39	56.2	15.1	14.9	3.2	0.0	0.0	0.0	0.0	0.0	10.6	0.02

4.2. Surface Texture

The surface texture of the studied rock samples from both Veria-Naousa and Gerania ophiolite complexes were investigated by using secondary electron images. The particle surfaces of the studied samples presented differences in their microtopography. Highly serpentinized rocks were characterized by smooth and glassy surface textures (Figure 6a,b). With the decreasing of serpentinization, the surfaces of rock particles appeared rougher, due to the presence of minerals of differential hardness, hence resulting in development of rugged and irregular surfaces (Figure 6c,d).

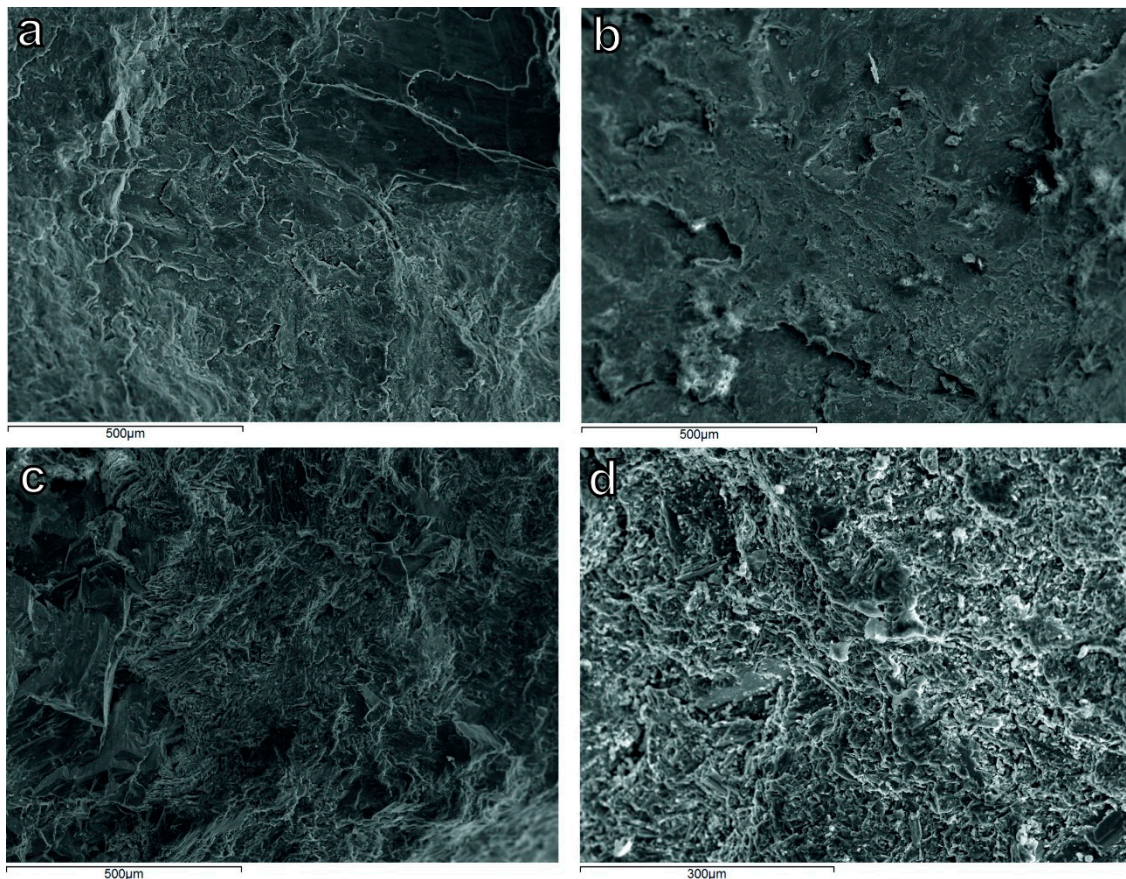


Figure 6. Secondary electron images showing the surface texture from representative ultramafic rock samples of Veria-Naousa and Gerania ophiolite complexes: (a) BE.01B serpentinized harzburgite; (b) BE.102 serpentinized lherzolite; (c) GE.30 lherzolite; and (d) GE.25-lherzolite.

4.3. Engineering Properties of Aggregates

4.3.1. Physical and Physicochemical Properties

The determined values of the moisture content, total porosity and soundness test of the rocks are listed in Table 2. The most serpentinized ultramafic samples showed higher values of physicochemical properties than those which contain lower percentages of serpentine. The moisture contents of the tested rocks varied from 0.04% to 2.58%, while the total porosity varied from 1.18% to 6.49%. The distribution of the soundness test results was substantially wide, ranging between 11.76% and 75.34%, where sample GE.28 appeared as the most resistant in excessive volume changes.

Table 2. Physical and physicochemical properties of the tested ultramafic rock samples (BE: Veria-Naousa ophiolite complex; GE: Gerania ophiolite complex).

Lithology	Samples	w (%)	n _t (%)	S (%)
Serpentinized harzburgite	BE.01B	2.58	6.49	75.34
Serpentinized harzburgite	BE.12B	2.18	3.30	25.20
Serpentinized lherzolite	BE.102	2.00	4.00	36.46
Serpentinized lherzolite	BE.103B	1.94	4.99	75.12
Serpentinized harzburgite	BE.122	1.25	3.21	30.00
Ol-orthopyroxenite	BE.67	0.41	1.18	12.90
Ol-orthopyroxenite	BE.67B	0.45	1.30	13.10
Serpentinized dunite	GE.17	0.90	1.56	14.62
Lherzolite	GE.25	0.04	0.78	17.49
Serpentinized lherzolite	GE.26	0.40	0.91	20.00
Harzburgite	GE.28	0.08	0.42	11.76
Lherzolite	GE.30	0.25	0.92	12.33
Lherzolite	GE.31	0.22	0.53	18.06
Lherzolite	GE.32	0.16	0.89	14.39
Lherzolite	GE.33	0.08	0.16	14.37
Dunite	GE.34	0.36	0.76	13.45
Serpentinized dunite	GE.37	0.43	0.76	22.82
Lherzolite	GE.39	0.25	0.89	18.02

4.3.2. Mechanical Properties

The mechanical properties of the studied ultramafic samples are listed in Table 3. Concerning the resistance in abrasion of the tested specimens, the LA values ranged from 14.22% to 32.00%. Both the UCS values ranging from 25.45 to 111.63 MPa, and the point load index $I_{s(50)}$ values ranging from 1.16 to 11.26 MPa showed a general antipathetic correlation with the serpentine contents.

Table 3. Mechanical properties of the tested ultramafic rock samples (BE: Veria-Naousa ophiolite complex; GE: Gerania ophiolite complex). UCS and $I_{s(50)}$ values are averaged based on 6 and 3 samples, respectively.

Lithology	Samples	LA (%)	UCS (MPa) (N = 6)	$I_{s(50)}$ (MPa) (N = 3)
Serpentinized harzburgite	BE.01B	32.00	51.00	2.76
Serpentinized harzburgite	BE.12B	25.16	55.40	1.88
Serpentinized lherzolite	BE.102	24.00	28.00	1.55
Serpentinized lherzolite	BE.103B	28.97	32.00	1.16
Serpentinized harzburgite	BE.122	25.51	25.45	3.00
Ol-orthopyroxenite	BE.67	14.22	85.70	11.26
Ol-orthopyroxenite	BE.67B	14.55	84.20	10.80
Serpentinized dunite	GE.17	20.30	93.05	3.46
Lherzolite	GE.25	15.89	79.00	6.92
Serpentinized lherzolite	GE.26	19.63	66.00	7.30
Harzburgite	GE.28	15.73	86.20	3.28
Lherzolite	GE.30	16.61	75.00	3.84
Lherzolite	GE.31	22.20	111.63	8.84
Lherzolite	GE.32	22.01	97.00	3.93
Lherzolite	GE.33	20.92	69.12	8.45
Dunite	GE.34	17.51	88.86	5.38
Serpentinized dunite	GE.37	17.36	100.00	4.22
Lherzolite	GE.39	19.76	95.39	4.61

5. Discussion

The petrographic analysis outlined above indicated that the studied ultramafic rocks have been variably affected by seafloor alteration processes. The results also demonstrated the importance of mineralogical and textural characteristics on their engineering performance as aggregate rocks. Several researchers have studied the effect of mineralogical composition (primary and secondary phases) on the engineering properties of rocks. Many of them have dealt with the influence of primary minerals, such

as biotite, quartz and K-feldspar on the mechanical properties of volcanic and granitic rocks, presenting no relationships between these primary minerals of the investigated rocks and their mechanical properties [8,11,53,54], while others have studied the negative influence of weathering/alteration on the engineering behavior of the tested rocks [5,22–24,55]. The generally lower hardness of the secondary minerals relative to the primary relics accompanied by new textures result in differential engineering behaviors, thus contributing to the weakness and easier deterioration of the rocks under stress and subsequently their gradually diminished in-service performance. This is assigned to the fact that the secondary minerals have substantially different physicochemical and physicochemical behavior compared with the primary ones, leading to the modification of rocks strength [2].

5.1. The Influence of Mineralogical Composition on the Physical and Physicochemical Properties

The studied ultramafic rocks from the Veria-Naousa and Gerania ophiolite complexes show considerable mineralogical and textural differences (Table 2). The most common statistical method for the investigation of the interdependence of the mineralogical composition of rocks and their physical and physicochemical properties is the regression analysis. In this study, the ratio of secondary to primary minerals (SEC/PR), which is thought to reflect the alteration degree of the rocks, was correlated with their physical and physicochemical properties. The total porosity, moisture content and soundness test values increased with the increased SEC/PR ratio (Figure 7a–c). The relationships between the physical and physicochemical properties and the SEC/PR ratio were expressed by the following linear and exponential equations:

$$w = 0.4965 \times \text{SEC/PR} + 0.2385, R^2 = 0.72 \text{ (Figure 7a)} \quad (1)$$

$$n_t = 1.1028 \times \text{SEC/PR} + 0.641, R^2 = 0.77 \text{ (Figure 7b)}, \quad (2)$$

$$S = 14.328e^{0.3299 \times (\text{SEC/PR})}, R^2 = 0.68 \text{ (Figure 7c)}. \quad (3)$$

Common secondary phases in ultramafic rocks include serpentine, talc, chlorite and magnetite. However, the investigated ultramafic rock samples included serpentine as a secondary mineral in dominant contents, while chlorite, talc, brucite and magnetite were presented in minor amounts. Very good positive correlations were observed when only serpentine contents were plotted against the porosity, moisture content and soundness test (Figure 7d–f), hence suggesting that this mineral played a determinant role among the secondary minerals and strongly controlled the SEC/PR ratio. The linear equations below fitted better the abundance of serpentine with the moisture content and the total porosity:

$$w = 0.0256 \times \text{serpentine} - 0.0122, R^2 = 0.77 \text{ (Figure 7d)}, \quad (4)$$

$$n_t = 0.0532 \times \text{serpentine} + 0.1978, R^2 = 0.72 \text{ (Figure 7e)} \quad (5)$$

The relationship between the abundance of serpentine and the soundness test was better described by the exponential equation:

$$S = 12.17e^{0.0169 \times \text{serpentine}}, R^2 = 0.72 \text{ (Figure 7f)}. \quad (6)$$

Similar correlations between the physical properties and the abundance of serpentine, expressed by the weathering grade, have also been observed in dunites from the Orhanli ophiolite complex in Turkey [56]. Regarding the soundness test, samples BE.01B and BE.103B presented the highest values (75.34% and 75.12%, respectively), as they displayed only mesh texture, which was responsible for their high S values. The existence of mesh texture led to more hydrous solutions (MgSO_4) to be flown along the pores and the planes of weakness of these ultramafic rocks, where the hydrous solution led to the expansion of these rocks during the stages of heating, due to the nature of this property. By ignoring these two samples with higher soundness values, the correlation diagrams between the ratio of SEC/PR and the soundness test as well as between the abundance of serpentine and the

soundness test could be better expressed by linear equations with $R^2 = 0.74$ and $R^2 = 0.73$, respectively (not shown).

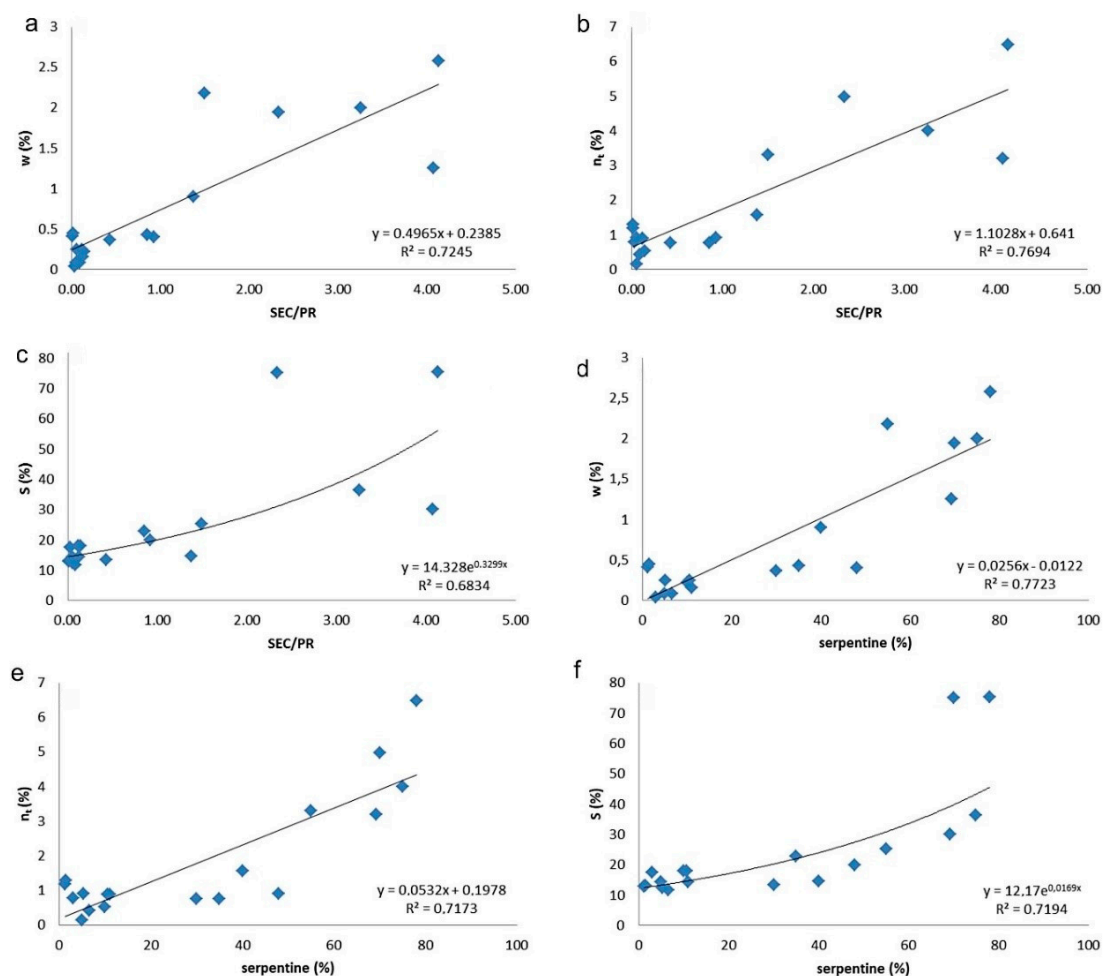


Figure 7. (a) The moisture content [w (%)] plotted against the ratio of secondary to primary minerals (SEC/PR) of all tested rock samples; (b) the total porosity [n_t (%)] plotted against the ratio of SEC/PR of all tested rock samples; (c) the soundness test [S (%)] plotted against the ratio of SEC/PR of all tested rock samples; (d) the moisture content [w (%)] plotted against the abundance of serpentine (%) of all tested rock samples; (e) the total porosity [n_t (%)] plotted against the abundance of serpentine (%) of all tested rock samples; and (f) the soundness test [S (%)] plotted against the abundance of serpentine (%) of all tested rock samples.

The secondary minerals were also correlated with the above physical and physicochemical properties and showed considerable but definitely less strong interrelationships with them. Poor correlations were observed when each primary mineral alone was plotted against the porosity, moisture content and soundness test (not shown).

Serpentinization is an important geochemical process accompanying the formation of the ocean floor [1]. During this process, anhedral or squat crystals of olivine and pyroxene transform into serpentine, a laminate, soft mineral, which belongs to the phyllosilicate subclass of minerals and forms smooth surfaces [57,58]. This crystallographic habit and physical properties of serpentine (i.e., platy shape, low hardness, excellent cleavage and smooth surfaces) have eventually an adverse effect on the quality of the ultramafic rocks, as it largely contributes to their deterioration during their in-service performance. Talc and chlorite have similar behavior to serpentine; however, their restricted appearance in the investigated rocks restrains them from having important detrimental contribution.

Magnetite is a typical secondary mineral forming during serpentinization. Its contribution to the performance of the rocks was investigated; however, poor correlations of its modal abundance with the above physical properties of rocks were observed (not shown). The increased ability of the rocks, which contain high contents of secondary minerals, to incorporate water can be explained by the fact that these platy or tabular secondary phases (i.e., serpentine, chlorite, talc and brucite) have the capability to adsorb water in their interlayered planes of their crystal structures. Moreover, these phases and particularly serpentine commonly form foliated masses, thus contributing to the development of more porous areas and to the enhanced adsorption of moisture.

The statistical significance of the above correlations was appraised using the *t*-test and the probability figure (*p*-value), as they do not present normal distributions. The significantly higher absolute values of the *t*-test than the critical *t*-table values, for confidence levels higher than 95%, as well as the very low *p*-values, strongly suggested the validity of the relationships, which were described by Equations (1)–(6) above, hence supporting the hypothesis of the influence of the ratio of SEC/PR and specifically the serpentine abundance on the physical and physicochemical properties of ultramafic rock samples (Table 4). Exceptionally, the correlation of SEC/PR ratio with moisture content (*w*) appeared valid for lower (and perhaps not acceptable) confidence levels; however, when only serpentine was considered, the correlation is statistically valid even for a confidence level of 99% (see Table 4).

Table 4. Paired *t*-test results for the statistical correlations of the SEC/PR ratio and the unit ratio of serpentine abundance with *w*, n_t and *S*. The listed critical *t*-table values are for the relevant freedom degrees (*dF*) and for confidence levels of 99% ($\alpha = 0.01$), 98% ($\alpha = 0.02$) and 95% ($\alpha = 0.05$).

Pairs	<i>t</i> -test	<i>dF</i>	<i>p</i> -value	<i>t</i> -tables		
				$\alpha = 0.01$	$\alpha = 0.02$	$\alpha = 0.05$
SEC/PR- <i>w</i>	1.552	17	0.1391	2.898	2.567	2.110
SEC/PR- n_t	-3.657	17	0.0019	2.898	2.567	2.110
SEC/PR- <i>S</i>	-5.436	17	0.00004	2.898	2.567	2.110
Serpentine- <i>w</i>	-3.334	17	0.039	2.898	2.567	2.110
Serpentine- n_t	-4.163	17	0.006	2.898	2.567	2.110
Serpentine- <i>S</i>	-5.372	17	0.00005	2.898	2.567	2.110

In this paper, we suggested that texture is another important factor for the engineering performance of the rocks. Variably serpentinized rocks show generally different textural features. Mesh textures are more abundant in the highly serpentinized samples, whereas granular, bastitic and ribbon textures predominate in the moderately serpentinized rocks. Unlike ribbon and bastitic textures, which display one direction of weakness along cleavage, the mesh textures in the highly serpentinized samples show multiple planes of weakness around the meshes. The different orientations of these planes are controlled by the shape of the mesh structures, forming a grid which is responsible for the formation of multiple open surfaces in the serpentinized ultramafic rocks, thus increasing their total porosity. These ultramafic rocks with high percentages of mesh textures allow more water or other hydrous solutions (e.g., the hydrous solution of $MgSO_4$ used for the soundness test) to flow easier along the open planes and pores. In this way, we interpreted that these rocks are more vulnerable to weathering, as larger amounts of salts can be crystallized and expand in the already weak surfaces.

5.2. The influence of Mineralogical Composition on the Mechanical Properties

Regression analysis was also used to investigate the interdependence of the mineralogical composition of ultramafic rocks with their mechanical properties. The SEC/PR ratio was plotted against the UCS, point load index and LA value. Strong negative trends were observed between the SEC/PR ratio and the UCS, as well as with the point load index, suggesting the negative influence of the secondary phases to the strength of the materials (Figure 8a,b). Moreover, the strong positive trend

between the SEC/PR ratio and the LA values also implied that increasing alteration resulted in less resistant rocks in abrasion (Figure 8c). The best-fit relationships between the mechanical properties and the SEC/PR ratio were expressed by the following equations:

$$\text{UCS} = 90.157e^{-0.262 \times (\text{SEC/PR})}, R^2 = 0.69 \text{ (Figure 8a),} \tag{7}$$

$$I_{s(50)} = -1.199\ln(\text{SEC/PR}) + 3.6794, R^2 = 0.57 \text{ (Figure 8b),} \tag{8}$$

$$\text{LA} = 2.8042 \times \text{SEC/PR} + 17.646, R^2 = 0.64 \text{ (Figure 8c).} \tag{9}$$

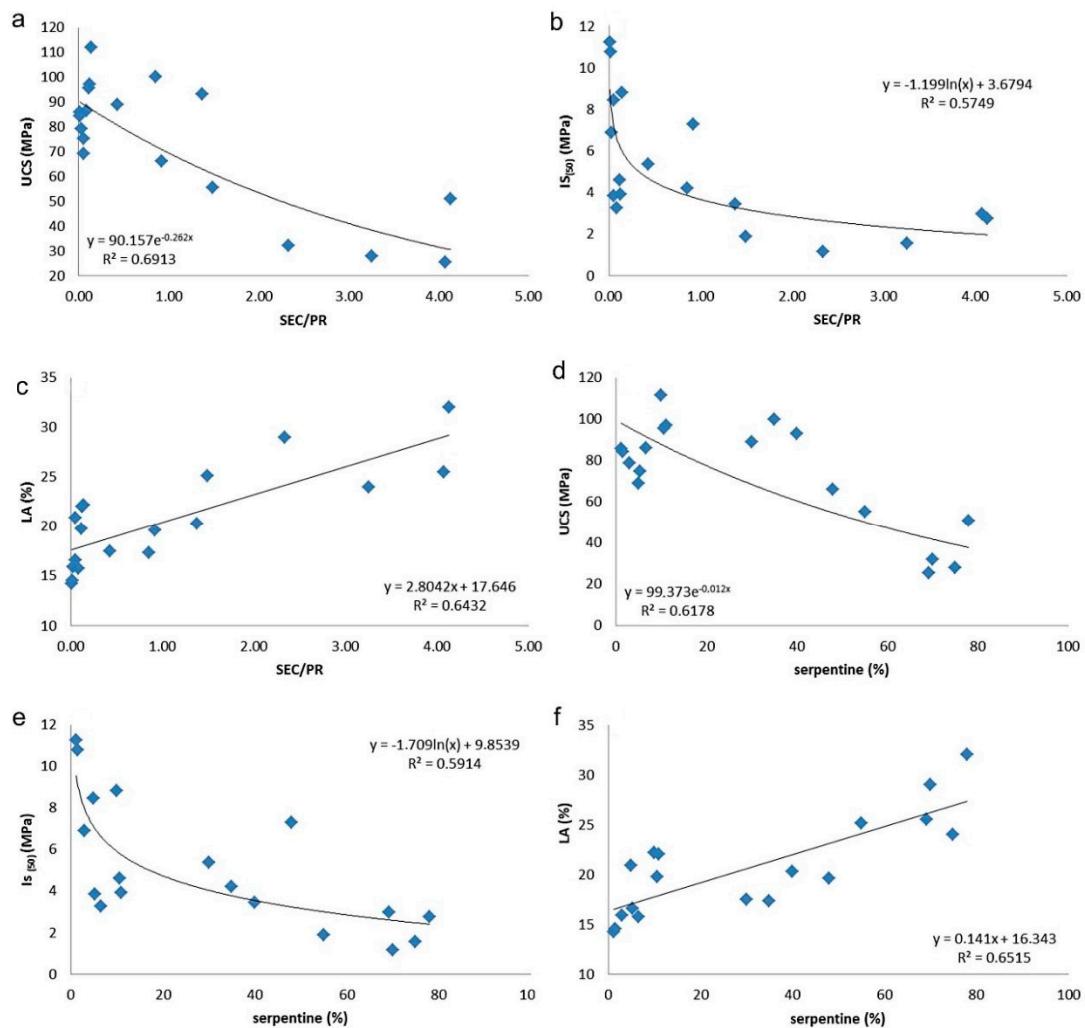


Figure 8. (a) The uniaxial compressive strength [UCS (MPa)] plotted against the ratio of secondary SEC/PR of all tested rock samples; (b) the point load test [$I_{s(50)}$ (MPa)] plotted against the ratio of SEC/PR of all tested rock samples; (c) the Los Angeles abrasion test [LA (%)] plotted against the ratio of SEC/PR of all tested rock samples; (d) the UCS (MPa) plotted against the abundance of serpentine (%) of all tested rock samples; (e) the point load test [$I_{s(50)}$ (MPa)] plotted against the abundance of serpentine (%) of all tested rock samples; (f) the Los Angeles abrasion test [LA (%)] plotted against the abundance of serpentine (%) of all tested rock samples.

Very good correlations were again observed when only serpentine contents alone were plotted against the UCS, point load index and LA value, which was again compatible with the determinant

role of this mineral. The exponential and logarithmic equations below fitted better the abundance of serpentine with the UCS values, (Figure 8d), the point load index (Figure 8e) and the LA values:

$$\text{UCS} = 99.373e^{-0.012 \times \text{serpentine}}, R^2 = 0.62 \text{ (Figure 8d)} \quad (10)$$

$$I_{s(50)} = -1.709 \ln \text{serpentine} + 9.8539, R^2 = 0.59 \text{ (Figure 8e)} \quad (11)$$

$$\text{LA} = 0.141 \times \text{serpentine} + 16.343, R^2 = 0.65 \text{ (Figure 8f)}. \quad (12)$$

The recommended relationship between the UCS and the abundance of serpentine was similar to the results of Diamantis et al. [59] who has shown a similar trend in peridotites from Central Greece, as well as similar to Undul and Tugrul [56] who have shown a similar trend in dunites from Northwestern Turkey. The secondary minerals were also correlated with the above mechanical properties and showed considerable but definitely less strong interrelationships with them. Poor correlations were observed when only each primary mineral was plotted against the values of the mechanical properties (not shown).

As has already mentioned, serpentine, chlorite and talc, due to their platy and layered characteristics, form foliated masses and mesh textures, which lead to the development of larger pores and open surfaces, expressed as the increased porosity. These areas disturb the cohesiveness of the structures, thus leading to mechanically weaker rocks. These interpretations are compatible with the results of Rigopoulos et al. [60], who have shown that after stress, the intragranular microcracks in mesh serpentine may organize in larger transgranular cracks. These cracks can propagate in the rocks at random orientations, along the preferential weak rims of the meshes, thus providing a plausible explanation for the detrimental effect of the mesh texture in the rocks, which leads to rocks of lower mechanical strength.

Despite the fact that studied dunites contain considerable amounts of serpentine (30.0–40.0%), they appear to be strong rocks. Therefore, one may wonder how the increased serpentine contents do not have the expected negative influence on these rocks. This seemingly inconsistent behavior in the mechanical properties of dunites can be explained from the fact that serpentine is mostly formed within the cracks of olivine, and therefore, a combination of hard olivine and soft serpentine network is formed nearly uniformly throughout the rock. Our interpretation is that the soft serpentine has the ability to act as a stress absorber among the hard olivine grains, also preventing the propagation of microcracks, which could lower the strength of the dunites.

The statistical validity of these correlations was tested with the aid of the *t*-test and the probability figure (*p*-value), as they do not present normal distributions. The significantly higher absolute values of the *t*-test than the critical *t*-table values, for confidence levels higher than 95%, as well as the very low *p*-values, strongly suggested the validity of the relationships described by Equations (7)–(12) above, hence supporting the hypothesis of the influence of the SEC/PR ratio and particularly of serpentine on the mechanical properties of ultramafic rock samples (Table 5).

Table 5. Paired *t*-test results for the statistical correlations of the SEC/PR ratio and unit ratio of serpentine abundance with UCS, $I_{s(50)}$ and LA. The listed critical *t*-table values are for the relevant freedom degrees (*dF*) and for confidence levels of 99% ($\alpha = 0.01$), 98% ($\alpha = 0.02$) and 95% ($\alpha = 0.05$).

Pairs	<i>t</i> -test	<i>dF</i>	<i>p</i> -value	<i>t</i> -tables		
				$\alpha = 0.01$	$\alpha = 0.02$	$\alpha = 0.05$
SEC/PR-UCS	−11.419	17	2.1×10^{-9}	2.898	2.567	2.110
SEC/PR- $I_{s(50)}$	−4.196	17	0.0006	2.898	2.567	2.110
SEC/PR-LA	−21.148	17	1.2×10^{-13}	2.898	2.567	2.110
Serpentine-UCS	−11.956	17	1.06×10^{-9}	2.898	2.567	2.110
Serpentine- $I_{s(50)}$	−6.241	17	9×10^{-6}	2.898	2.567	2.110
Serpentine-LA	−18.182	17	1.41×10^{-12}	2.898	2.567	2.110

In the studied ultramafic rocks, the soft nature and the phyllosilicate crystal habit of the secondary minerals were reflected in the external microtopography of the aggregate particles. Unlike the rocks with relatively higher amounts of primary relic minerals, which show substantially higher microtopography, highly serpentinized specimens showed smooth surfaces and low microtopography (Figure 6). For example, samples, such as BE.01 and BE.102, which contain high percentages of serpentine unevenly distributed in the rocks, presented low microtopography. On the other hand, samples, such as GE.28 and GE.37, which contain low to moderate serpentine percentages occurring uniformly in the rocks, presented high microtopography. This affects the selection of the aggregates in a number of applications, where angular grains (i.e., high microtopography) are required. We can mention the concrete aggregates as examples, which form better bonds with the cement paste when they show rough surfaces [5], as well as the ballast (road or railway) aggregates where angular particles presumably show better locking and hence stability [61]. The coexistence of soft (serpentine, talc, chlorite, brucite) and hard minerals (olivine, orthopyroxene, clinopyroxene, spinel and magnetite) forms rather angular surfaces with rough projections, because the first are easier weathered relative to the latter. Therefore, low to moderately altered ultramafic rocks can be even more advantageous relative to totally fresh ones, due to the fact the preferential weathering of the soft minerals assists in the renewal of the aggregate microroughness when these rocks are in service [2]. This improves the adhesion between the tires and the road surface, principally at low speeds [62].

6. Conclusions

This paper investigated the influence of the mineralogical composition and textural characteristics of the ultramafic rocks on their engineering properties. With the increasing of alteration, the physicochemical and mechanical properties of the ultramafic rocks were aggravated. The soft and platy nature of serpentine, as well as the formation of mesh textures, is a critical factor for the development of extensive porous areas, which are weak. Moreover, water or hydrous solutions (followed by salt crystallization) can easily flow along them, further reducing the durability of the rocks. Pre-existing weak surfaces in highly serpentinized rocks can be combined after stress to larger and longer cracks, therefore contributing to the low mechanical in-service performance of the ultramafic aggregates. Exceptionally in dunites, the negative consequences of serpentinization are partly counterbalanced by the homogeneous distribution of the soft serpentine along cracks of the hard olivine. This effect prevents the formation and propagation of new cracks, as the serpentine acts as a stress absorber, thus creating a mechanically stronger system relative to other ultramafic rocks with similar degrees of alteration. Moreover, moderate degrees of alteration can also be beneficial for the development of adequate microtopography (and angularity) in the external surface of aggregates, due to the preferential weathering of the soft over the hard, relic minerals.

Author Contributions: P.P.G. participated in the fieldwork, the elaboration of laboratory tests, the interpretation of the results, coordinated the research and wrote the paper; P.P. (Petros Petrounias) participated in the fieldwork, the elaboration of laboratory tests, the interpretation of the results and wrote the paper; A.R. participated in the fieldwork and performed the SEM work; B.T. participated in the fieldwork, in the interpretation of the results and in writing the paper; P.M.S. participated in the elaboration of the laboratory tests and the interpretation of the results; P.P. (Panagiotis Pomonis) participated in the fieldwork, in the interpretation of the results and in writing the paper; and K.H. participated in the interpretation of the results.

Acknowledgments: We express our thanks to A.K. Seferlis from the Laboratory of Electron Microscopy and Microanalysis, University of Patras for his assistance with the microanalyses and SEM micrographs. Critical reviews from the anonymous reviewers have substantially improved the manuscript and are gratefully acknowledged.

Conflicts of Interest: The authors declare no conflicts of interest.

References

1. Escartin, J.; Hirth, G.; Evans, B. Strength of slightly serpentinized peridotites: Implications for the tectonics of oceanic lithosphere. *Geology* **2001**, *29*, 1023–1026. [[CrossRef](#)]

2. Rigopoulos, I.; Tsikouras, B.; Pomonis, P.; Hatzipanagiotou, K. The influence of alteration on the engineering properties of dolerites: The example from the Pindos and Vourinos ophiolites (northern Greece). *Int. J. Rock Mech. Min. Sci.* **2010**, *47*, 69–80. [[CrossRef](#)]
3. Rigopoulos, I.; Tsikouras, B.; Pomonis, P.; Hatzipanagiotou, K. Assessment of the engineering behavior of ultramafic and mafic rocks using chemical indices. *Eng. Geol.* **2015**, *196*, 222–237. [[CrossRef](#)]
4. Petrounias, P.; Rogkala, A.; Kalpogiannaki, M.; Tsikouras, B.; Hatzipanagiotou, K. Comparative study of physico-mechanical properties of ultrabasic rocks (Veria-Naousa ophiolite) and andesites from central Macedonia (Greece). *Bull. Geol. Soc. Gr.* **2016**, *50*, 1989–1998.
5. Petrounias, P.; Giannakopoulou, P.P.; Rogkala, A.; Stamatis, P.M.; Tsikouras, B.; Papoulis, D.; Lampropoulou, P.; Hatzipanagiotou, K. The Influence of Alteration of Aggregates on the Quality of the Concrete: A Case Study from Serpentinities and Andesites from Central Macedonia (North Greece). *Geosciences* **2018**, *8*, 115. [[CrossRef](#)]
6. Smith, M.R.; Collis, L. *Aggregates: Sand, Gravel and Crushed Rock Aggregates for Construction Purposes*; Special Publications 17; Geological Society: London, UK, 2001.
7. Pomonis, P.; Rigopoulos, I.; Tsikouras, B.; Hatzipanagiotou, K. Relationships between petrographic and physico-mechanical properties of basic igneous rocks from the Pindos ophiolitic complex, NW Greece. *Bull. Geol. Soc. Greece* **2007**, *2*, 947–958. [[CrossRef](#)]
8. Yilmaz, M.; Goktan, R.M.; Kibici, Y. Relations between some quantitative petrographic characteristics and mechanical strength properties of granitic building stones. *Int. J. Rock Mech. Min. Sci.* **2011**, *48*, 506–513. [[CrossRef](#)]
9. Yilmaz, M.; Turgul, A. The effect of different sandstone aggregates on concrete strength. *Constr. Build. Mater.* **2012**, *35*, 294–303. [[CrossRef](#)]
10. Giannakopoulou, P.P.; Tsikouras, B.; Hatzipanagiotou, K. The interdependence of mechanical properties of ultramafic rocks from Gerania ophiolitic complex. *Bull. Geol. Soc. Greece* **2016**, *50*, 1829–1837. [[CrossRef](#)]
11. Tandon, R.S.; Gupta, V. The control of mineral constituents and textural characteristics on the petrophysical and mechanical (PM) properties of different rocks of the Himalaya. *Eng. Geol.* **2013**, *153*, 125–143. [[CrossRef](#)]
12. Ündül, Ö. Assessment of mineralogical and petrographic factors affecting petro-physical properties, strength and cracking processes of volcanic rocks. *Eng. Geol.* **2016**, *210*, 10–22. [[CrossRef](#)]
13. Cowie, S.; Walton, G. The effect of mineralogical parameters on the mechanical properties of granitic rocks. *Eng. Geol.* **2018**. [[CrossRef](#)]
14. Ioannou, I.; Fournari, R.; Petrou, M.F. Testing the Soundness of aggregates using different methodologies. *Constr. Build. Mater.* **2013**, *40*, 604–610. [[CrossRef](#)]
15. Arel, E.; Turgul, A. Weathering and its relation to geomechanical properties of Gavusbasi granitic rocks in northwestern Turkey. *Bull. Eng. Geol. Environ.* **2001**, *60*, 123–133.
16. Ceryan, S.; Tudes, S.; Ceryan, N. Influence of weathering on the engineering properties of Harsit granitic rocks (NE Turkey). *Bull. Eng. Geol. Environ.* **2008**, *67*, 97–104. [[CrossRef](#)]
17. Das, A.; Krishnaswami, S.; Sarin, M.M.; Pande, K. Chemical weathering in the Krishna Basin and Western Ghats of the Deccan Traps, India: Rates of basalt weathering and their controls. *Geochim. Cosmochim. Acta* **2005**, *69*, 2067–2084. [[CrossRef](#)]
18. Orhan, M.; Isik, N.; Topal, T.; Ozer, M. Effect of weathering on the geomechanical properties of andesite, Ankara-Turkey. *Environ. Geol.* **2006**, *50*, 85–100. [[CrossRef](#)]
19. Cascini, L.; Nocera, S.; Critelli, S.; Gulla, G.; Matano, F. Weathering and land sliding in Sila Massif gneiss (Northern Calabria, Italy). In Proceedings of the 7th International Congress-International Association of Engineering Geology, Rotterdam, The Netherlands, 5–9 September 1994; pp. 1613–1622.
20. Price, J.R.; Velbel, M.A. Chemical weathering indices applied to weathering profiles developed on heterogeneous felsic metamorphic parent rocks. *Chem. Geol.* **2003**, *202*, 397–416. [[CrossRef](#)]
21. Augustin, N.; Lackschewitz, K.S.; Kuhn, T.; Devey, C.W. Mineralogical and chemical mass changes in mafic and ultramafic rocks from the Logatchev hydrothermal field (MAR 15°N). *Mar. Geol.* **2008**, *256*, 18–29. [[CrossRef](#)]
22. Diamantis, K.; Gartzos, E.; Migiros, G. Study on uniaxial compressive strength, point load strength index, dynamic and physical properties of serpentinites from Central Greece: Test results and empirical relations. *Eng. Geol.* **2009**, *108*, 199–207. [[CrossRef](#)]

23. Rigopoulos, I.; Tsikouras, B.; Pomonis, P.; Hatzipanagiotou, K. The impact of petrographic characteristics on the engineering properties of ultrabasic rocks from northern and central Greece. *Q. J. Eng. Geol. Hydrogeol.* **2012**, *45*, 423–433. [[CrossRef](#)]
24. Undul, O.; Turgul, A. The influence of weathering on the engineering properties of dunites. *Rock Mech. Rock Eng.* **2012**, *45*, 225–239. [[CrossRef](#)]
25. Deschamps, F.; Godard, M.; Guillot, S.; Hattori, K. Geochemistry of subduction zone serpentinites: A review. *Lithos* **2013**, *178*, 96–127. [[CrossRef](#)]
26. Shervais, J.W.; Kolesar, P.; Andreasen, K. A field and chemical study of serpentinitization—Stonyford, California: Chemical flux and mass balance. *Int. Geol. Rev.* **2005**, *47*, 1–23. [[CrossRef](#)]
27. Malvoisin, B. Mass transfer in the oceanic lithosphere: Serpentinization is not isochemical. *Earth Planet. Sci. Lett.* **2015**, *430*, 75–85. [[CrossRef](#)]
28. Sleep, N.H.; Meibom, A.; Fridriksson, T.; Coleman, R.G.; Bird, D.K. H₂-rich fluids from serpentinitization: Geochemical and biotic implications. *Proc. Natl. Acad. Sci. USA* **2004**, *101*, 12818–12823. [[CrossRef](#)] [[PubMed](#)]
29. Reynard, B. Serpentine in active subduction zones. *Lithos* **2013**, *178*, 171–185. [[CrossRef](#)]
30. Guillot, S.; Hattori, K.H.; Sigoyer, J.; Nagler, T.; Auzende, A.L. Evidence of hydration of the mantle wedge and its role in the exhumation of eclogites. *Earth Planet. Sci. Lett.* **2001**, *193*, 115–127. [[CrossRef](#)]
31. Maffione, M.; Thieulot, C.; Hinsbergen, D.J.J.; Morris, A.; Plümpner, O.; Spakman, W. Dynamics of intraoceanic subduction initiation: 1. oceanic detachment fault inversion and the formation of supra-subduction zone ophiolites. *Geochem. Geophys.* **2015**, *16*, 1753–1770. [[CrossRef](#)]
32. Guillot, S.; Schwartz, S.; Reynard, B.; Agard, P.; Prigent, C. Tectonic significance of serpentinites. *Tectonophysics* **2015**, *646*, 1–19. [[CrossRef](#)]
33. Mercier, J.; Vergely, P.; Bebien, J. Les ophiolites helléniques “obductées” au Jurassique supérieures sont-elles les vestiges d’ un océan téthysien ou d’ une margine péri-européenne. *C. R. Somm. Soc. Geol. Fr.* **1975**, *17*, 108–112.
34. Saccani, E.; Photiades, A.; Santato, A.; Zeda, O. New evidence for supra-subduction zone ophiolites in the Vardar zone of northern Greece: Implications for the tectonomagmatic evolution of the Vardar oceanic basin. *Ophioliti* **2008**, *33*, 65–85.
35. Rogkala, A.; Petrounias, P.; Tsikouras, B.; Hatzipanagiotou, K. Petrogenetic significance of spinel from serpentinitized peridotites from Veria-Naousa ophiolite. *Bull. Geol. Soc. Gr.* **2016**, *50*, 1999–2008.
36. Rogkala, A.; Petrounias, P.; Tsikouras, B.; Hatzipanagiotou, K. New occurrence of pyroxenites in the Veria-Naousa ophiolite (North Greece): Implications on their origin and petrogenetic evolution. *Geosciences* **2017**, *7*, 92. [[CrossRef](#)]
37. Brunn, J.H. *Geological Map of Greece, Veroia Sheet, 1:50,000*; IGME: Athens, Greece, 1982.
38. Clément, B. Découverte d’ un flysch éocène en Béotie (Grèce continentale). *C. R. Acad. Sci.* **1971**, *272*, 791–792.
39. Bornovas, J. *Geological Map of Greece, Kapareli Sheet, 1:50,000*; IGME: Athens, Greece, 1981.
40. Clément, B. Evolution Géodynamique d’ un Secteur des Hellénides Internes: L’ Attique-Béotie (Grèce Continentale). Ph.D. Thesis, University Lille, Lille, France, 1983.
41. Vacondios, I. Etude Métallogénique des Chromites Liées aux Ophiolites de Type Méditerranéenne Occidentale ou orientale: Le chromite de Tinos et des Gerannes. Ph.D. Thesis, University of Patras, Patras, Greece, 1997.
42. Danelian, T.; Robertson, A.H.F. Palaeogeographic implications of the age of radiolarian-rich sediments in Beotia (Greece). *Bull. Geol. Soc. Gr.* **1998**, *32*, 21–29.
43. *Part 1: Composition, Specifications and Conformity Criteria for Common Cements*; EN 932-1; European Standard: Pilsen, Czech Republic, 2011.
44. *Part 3: Procedure and Terminology for Simplified Petrographic Description*; EN 932; European Standard: Pilsen, Czech Republic, 1996.
45. Bish, D.L.; Post, J.E. Quantitative mineralogical analysis using the Rietveld full pattern fitting method. *Am. Mineral.* **1993**, *78*, 932–940.
46. BSI (British Standards Institution). Part 1: Methods for Determination of Particle Size and Shape. In *Methods for Sampling and Testing of Mineral Aggregates, Sands and Fillers*; BSI: London, UK, 1975.
47. AASHTO (American Association of State Highway and Transportation Officials). *Standard Method of Test for Total Evaporable Moisture Content of Aggregate by Drying*; T255; AASHTO: Washington, DC, USA, 2000.

48. Brown, E. (Ed.) ISRM Suggested Methods. In “Rock Characterization Testing and Monitoring”; Pergamon Press: Oxford, UK, 1981.
49. ASTM. *Resistance to Abrasion of Small-Size Coarse Aggregate by Use of the Los Angeles Machine*; ASTM C-131; American Society for Testing and Materials: Philadelphia, PA, USA, 1989.
50. *Tests for Thermal and Weathering Properties of Aggregates—Part 2: Magnesium Sulfate Test*; EN 1367-2; European Committee for Standardization: Brussels, Belgium, 1999.
51. ASTM. *Standard Test Method of Unconfined Compressive Strength of Intact Rock Core Specimens*; ASTM D-2938; American Society for Testing and Materials: Philadelphia, PA, USA, 1986.
52. ISRM Suggested method for determining point load strength. *Int. J. Rock Mech. Min. Sci. Geomech. Abstr.* **1985**, *22*, 51–62.
53. Zorlu, K.; Ulusay, R.; Ocakoglu, F.; Gokceoglu, C.; Sommez, H. Predicting intact rock properties of selected sandstones using petrographic thin-section data. *Int. J. Rock Mech. Min. Sci.* **2004**, *41*, 93–98. [[CrossRef](#)]
54. Sajid, M.; Coggan, J.; Arif, M.; Andersen, J.; Rollinson, G. Petrographic features as an effective indicator for the variation in strength of granites. *Eng. Geol.* **2016**, *202*, 44–54. [[CrossRef](#)]
55. Christensen, N.I. Serpentinities, peridotites and seismology. *Int. Geol. Rev.* **2004**, *46*, 795–816. [[CrossRef](#)]
56. Undul, O.; Turgul, A. On the variations of geo-engineering properties of dunites and diorites related to weathering. *Environ. Earth Sci.* **2016**, *75*, 1326. [[CrossRef](#)]
57. Frost, B.R.; Beard, J.S. On silica activity and serpentinization. *J. Petrol.* **2007**, *48*, 1351–1368. [[CrossRef](#)]
58. Evans, B.W. Control of the products of serpentinization by the $\text{Fe}^{2+}\text{Mg}_{-1}$ exchange potential of olivine and orthopyroxene. *J. Petrol.* **2008**, *49*, 1873–1887. [[CrossRef](#)]
59. Diamantis, K.; Gartzos, E.; Migiros, G. Influence of petrographic characteristics on physico-mechanical properties of ultrabasic rocks from central Greece. *Bull. Eng. Geol. Environ.* **2014**, *73*, 1273–1292. [[CrossRef](#)]
60. Rigopoulos, I.; Tsikouras, B.; Pomonis, P.; Hatzipanagiotou, K. Microcracks in ultrabasic rocks under uniaxial compressive stress. *Eng. Geol.* **2011**, *117*, 104–113. [[CrossRef](#)]
61. Koohmishi, M.; Palassi, M. Evaluation of morphological properties of railway ballast particles by image processing method. *Transp. Geot.* **2017**, *12*, 15–25. [[CrossRef](#)]
62. Sabey, B.E. Road surface characteristics and skidding resistance. *J. Br. Granite Whinstone Fed.* **1965**, *5*, 7–20. [[CrossRef](#)]

